ACS Chemical Neuroscience

pubs.acs.org/chemneuro
Research Article

Increased Expression of VCAM1 on Brain Endothelial Cells Drives Blood–Brain Barrier Impairment Following Chronic Cerebral Hypoperfusion

Huiwen Zhang, Junkui Shang, Wei Li, Dandan Gao, and Jiewen Zhang*

Cite This: ACS Chem. Neurosci. 2024, 15, 2028–2041
Read Online

ABSTRACT: Chronic cerebral hypoperfusion (CCH)-triggered blood–brain barrier (BBB) dysfunction is a core pathological change occurring in vascular dementia (VD). Despite the recent advances in the exploration of the structural basis of BBB impairment and the routes of entry of harmful compounds after a BBB leakage, the molecular mechanisms inducing BBB impairment remain largely unknown in terms of VD. Here, we employed a CCH-induced VD model and discovered increased vascular cell adhesion molecule 1 (VCAM1) expression on the brain endothelial cells (ECs). The expression of VCAM1 was directly correlated with the severity of BBB impairment. Moreover, the VCAM1 expression was associated with different regional white matter lesions. Furthermore, a compound that could block VCAM1 activation, K-7174, was also found to alleviate BBB leakage and protect the white matter integrity, whereas pharmacological manipulation of the BBB leakage did not affect the VCAM1 expression. Thus, our results demonstrated that VCAM1 is an important regulator that leads to BBB dysfunction following CCH. Blocking VCAM1-mediated BBB impairment may thus offer a new strategy to treat CCH-related neurodegenerative diseases.

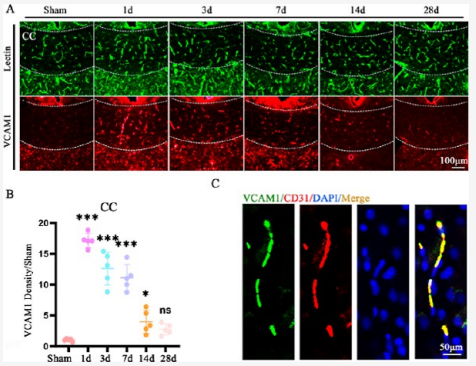

KEYWORDS: *vascular dementia, blood–brain barrier, VCAM1, chronic cerebral hypoperfusion, white matter lesions, endothelial inflammation*

1. INTRODUCTION

The blood–brain barrier (BBB) prevents neurotoxic plasma components, blood cells, and pathogens from entering the brain.[1] Meanwhile, the BBB plays a crucial role in regulating the transport of molecules into and out of the central nervous system (CNS). This regulation is essential for maintaining the tightly controlled chemical composition of the neuronal milieu, which is necessary for proper neuronal functioning.[2,3] Mounting evidence suggests that BBB dysfunction is pivotal in the pathogenesis of vascular dementia (VD),[4] which imposes a serious health burden on the society.[5] The BBB dysfunction and white matter lesions (WMLs) are two primary pathological changes as a result of chronic cerebral hypoperfusion (CCH) in VD. The BBB impairment is the key factor linking CCH to WMLs in VD. In VD, BBB impairment is more severe in areas near the WMLs than in areas of apparently normal white matter.[6,7] Consequently, considerable research has been directed toward elucidating the pathological alterations of the BBB in VD. The anatomical structure of the BBB is composed of endothelial cells (ECs), pericytes, astrocytic end-foot, and junctional complexes including tight junctions and adherens junctions.[2] Several important cellular mechanisms have been discovered during the exploration of the structural changes of the BBB in VD, including EC dysfunction, pericyte loss, and junctional complexes remodeling. Furthermore, research has shown that circulating pathogens and other potentially toxic substances can enter the brain through two primary pathways: the tight junctions between ECs and the endocytosis of ECs.[8] However, these studies have primarily focused on the structural aspects of BBB dysfunction and pathways of harmful material, neglecting an in-depth exploration of the underlying trigger factors. Consequently, the molecular mechanisms underlying BBB dysfunction remain largely elusive.

The function of BBB is highly dependent on ECs.[9] The combination of physical barrier properties (i.e., tight junctions and low transcytosis), molecular barrier properties (i.e., efflux transporters, specific metabolism, and low leukocyte adhesion molecule), as well as specific transporters to deliver required nutrients allows the ECs to tightly regulate the CNS homeostasis.[10] Impaired EC function allows toxic substances from the blood to enter the brain, resulting in irreversible brain

Received: January 18, 2024
Revised: April 19, 2024
Accepted: April 24, 2024
Published: May 6, 2024

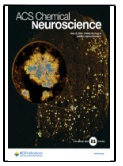

https://doi.org/10.1021/acschemneuro.4c00039
ACS Chem. Neurosci. 2024, 15, 2028–2041

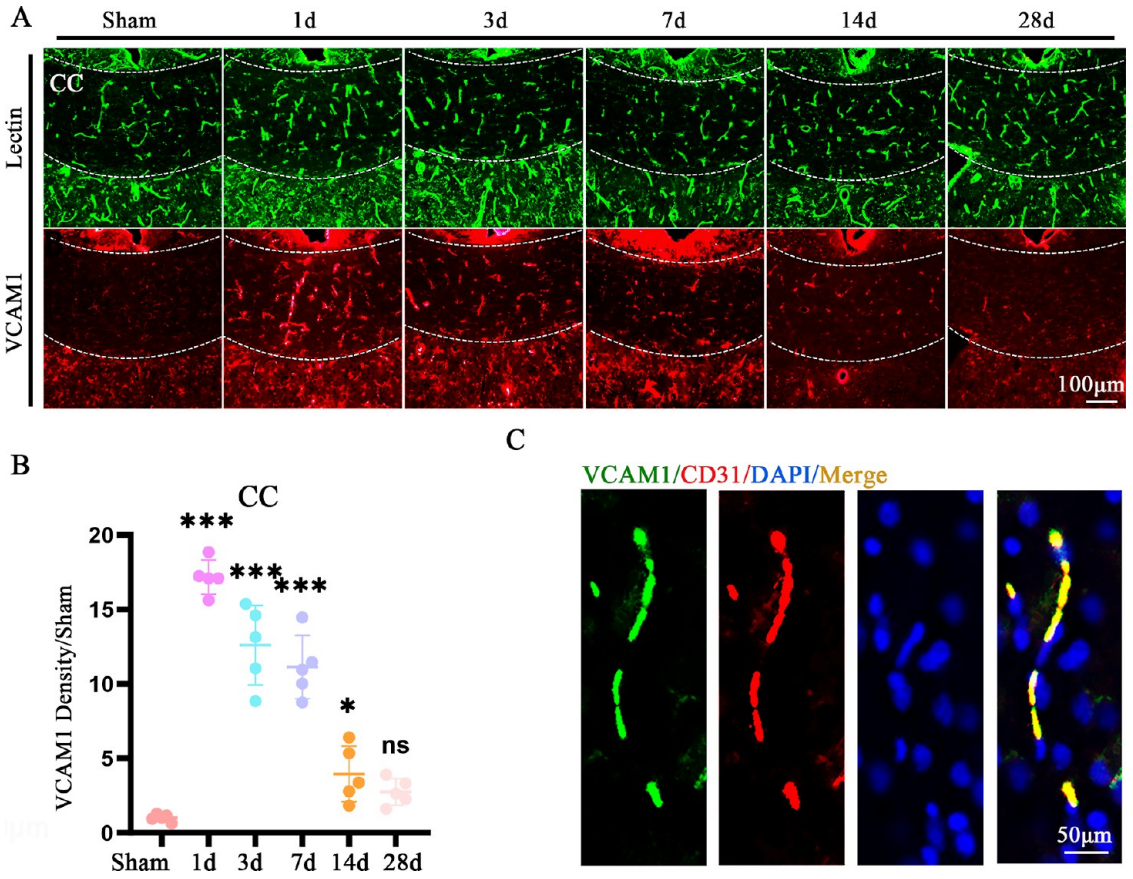

Figure 1. Vascular cell adhesion molecule 1 (VCAM1) upregulates on endothelial cells (ECs) of cerebral microvessels after chronic cerebral hypoperfusion (CCH). (A,B) Immunofluorescence staining and quantification of VCAM1 on blood vessels at different time points in the corpus callosum (CC); blood vessels were labeled by lectin (lectin, green; VCAM1, red; the region within the white dashed box is CC; $n = 5$). (C) Triple staining for CD31, VCAM1, and DAPI demonstrated VCAM1 colocalization with ECs (CD31, red; VCAM1, green; and DAPI, blue). Scales are shown in the figure; ns, not significant; *$p < 0.05$, **$p < 0.01$, and ***$p < 0.001$ compared to the sham group; one-way analysis of variance (ANOVA), followed by Dunnett's post hoc test.

injury. Throughout the development of VD, a series of molecular cascade responses associated with ECs closely correlate with the onset of cerebrovascular injury and VD.[11] Hence, we postulated that EC dysfunction serves as the central trigger for BBB impairment in VD. Elevated levels of plasma-soluble vascular cell adhesion molecule 1 (VCAM1) serve as a marker of endothelial dysfunction in both the brain and systemic circulation.[12] VCAM1, a member of the immunoglobulin superfamily, functions as a crucial cell adhesion molecule prominently expressed on the surface of activated ECs. VCAM1 upregulates the inflammatory response in ECs and interacts with the integrin receptor alpha4 beta1 (VLA4), facilitating the recognition of circulating lymphocytes and monocytes and mediating their entry into the brain parenchyma, thus promoting inflammation.[13] Endothelial inflammation driven by VCAM1 represents a typical pathological alteration with EC injury.[8] Following the reduction of cerebral blood flow, a plethora of proinflammatory factors, mediators, and chemokines are released, consequently inducing the expression of VCAM1, thereby amplifying the inflammatory response.[14] Additionally, studies have reported a negative correlation between soluble VCAM1 levels in the blood and cognitive impairment as well as cerebrovascular dysfunction.[12] Thus, we postulate that VCAM1 may play a significant role in inducing BBB dysfunction following CCH.

2. RESULTS

2.1. VCAM1 Upregulates on ECs of Cerebral Microvessels Following CCH. VCAM1 is a cell adhesion molecule specifically expressed on ECs, facilitating the entry of immune cells into the brain parenchyma.[15] This study first investigated VCAM1 expression on cerebral blood vessels following CCH. VCAM1 expression was low in the blood vessels of sham mice (Figure 1A,B), consistent with previous findings.[16] However, 1 day following CCH, a significant increase in VCAM1 expression was observed on CC microvessels compared to sham mice. To investigate whether VCAM1 upregulation occurred only in the acute phase, we extended the observation period to 28 days. Subsequently, we continuously observed increased VCAM1 expression from 3 to 28 days following CCH. However, the expression gradually decreased from 3 to 28 days compared to 1 day post-surgery (Figure 1A,B). Similar changes in VCAM1 expression were observed in cingulated gyrus (Cing) and external capsule (EC) microvessels (Figure S1). To further validate VCAM1 expression on brain ECs, we performed costaining of CD31 and VCAM1 on brain microvessels. VCAM1 colocalized with CD31 in the CC (Figure 1C), suggesting that CCH induces VCAM1 upregulation on the brain ECs.

2.2. BBB Breakdown Severely Following CCH. BBB tightly regulates substance exchange between the blood and the CNS, thereby maintaining the brain parenchymal micro-

https://doi.org/10.1021/acschemneuro.4c00039
ACS Chem. Neurosci. 2024, 15, 2028−2041

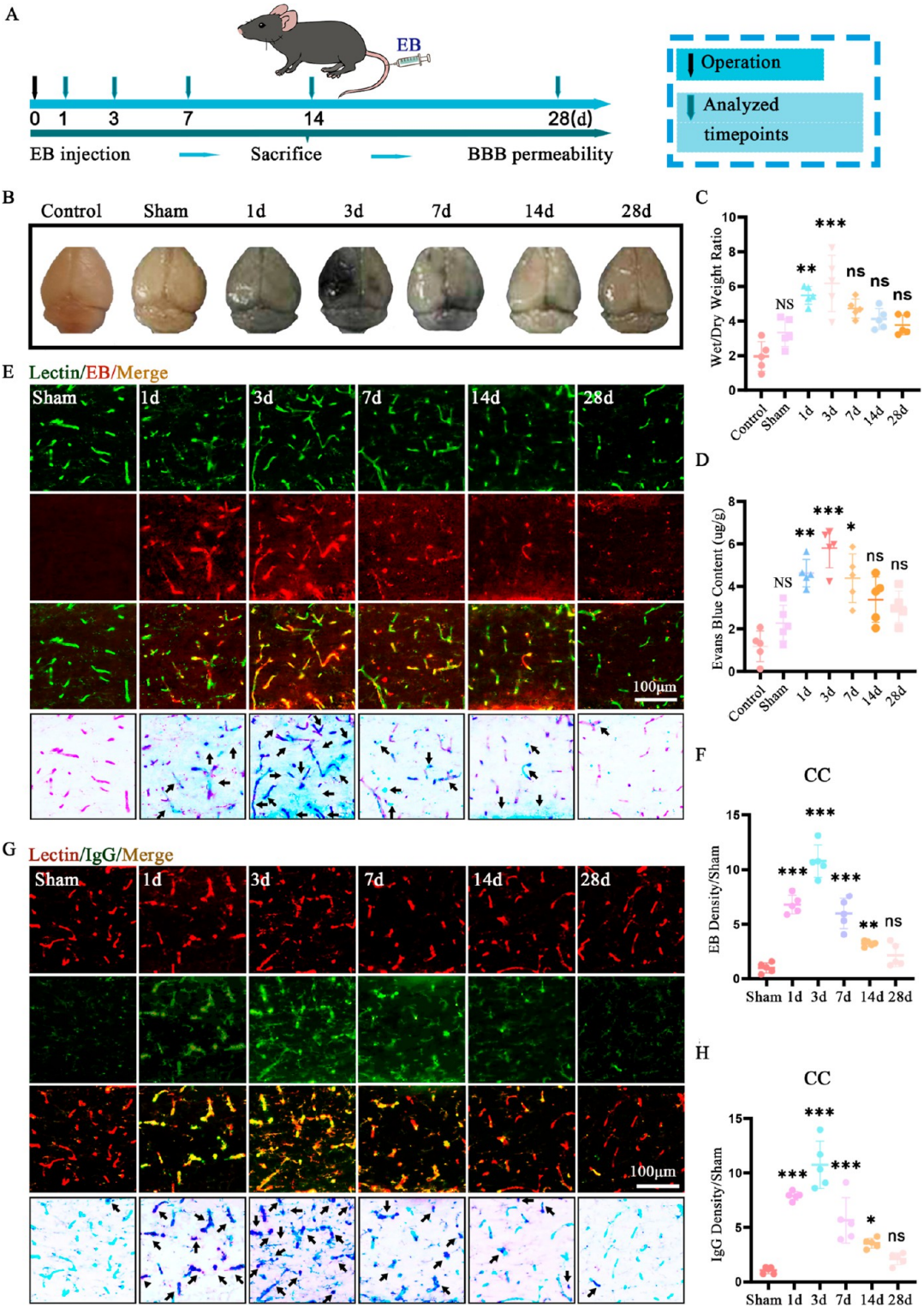

Figure 2. BBB breakdown severely following CCH. (A) Schematic diagram illustrating the detection of BBB permeability. (B) Gross anatomical changes in the brain in the control group, sham group, and 1, 3, 7, 14, and 28 days groups after EB injection. (C) Time-dependent change in the brain wet/dry weight ratio in the control group, sham group, and 1, 3, 7, 14, and 28 days groups following CCH (n = 5). (D) Quantification of EB content in the control group, sham group, and 1, 3, 7, 14, and 28 days groups following CCH (n = 5). (E,F) Fluorescence staining and quantification of EB leakage at different time points in the CC; blood vessels were labeled by lectin (lectin, green; EB, red; and arrows indicate EB leaking out of the blood vessels, n = 5). (G,H) Fluorescence staining and quantification of IgG accumulation at different time points in the CC; blood vessels were labeled by lectin (lectin, red; IgG, green; and arrows indicate IgG leaking out of the blood vessels, n = 5). Scales are shown in the figure; NS, not significant compared to the control group; ns, not significant; *p < 0.05, **p < 0.01, and ***p < 0.001 compared to the sham group; one-way ANOVA, followed by Dunnett's post hoc test.

https://doi.org/10.1021/acschemneuro.4c00039
ACS Chem. Neurosci. 2024, 15, 2028−2041

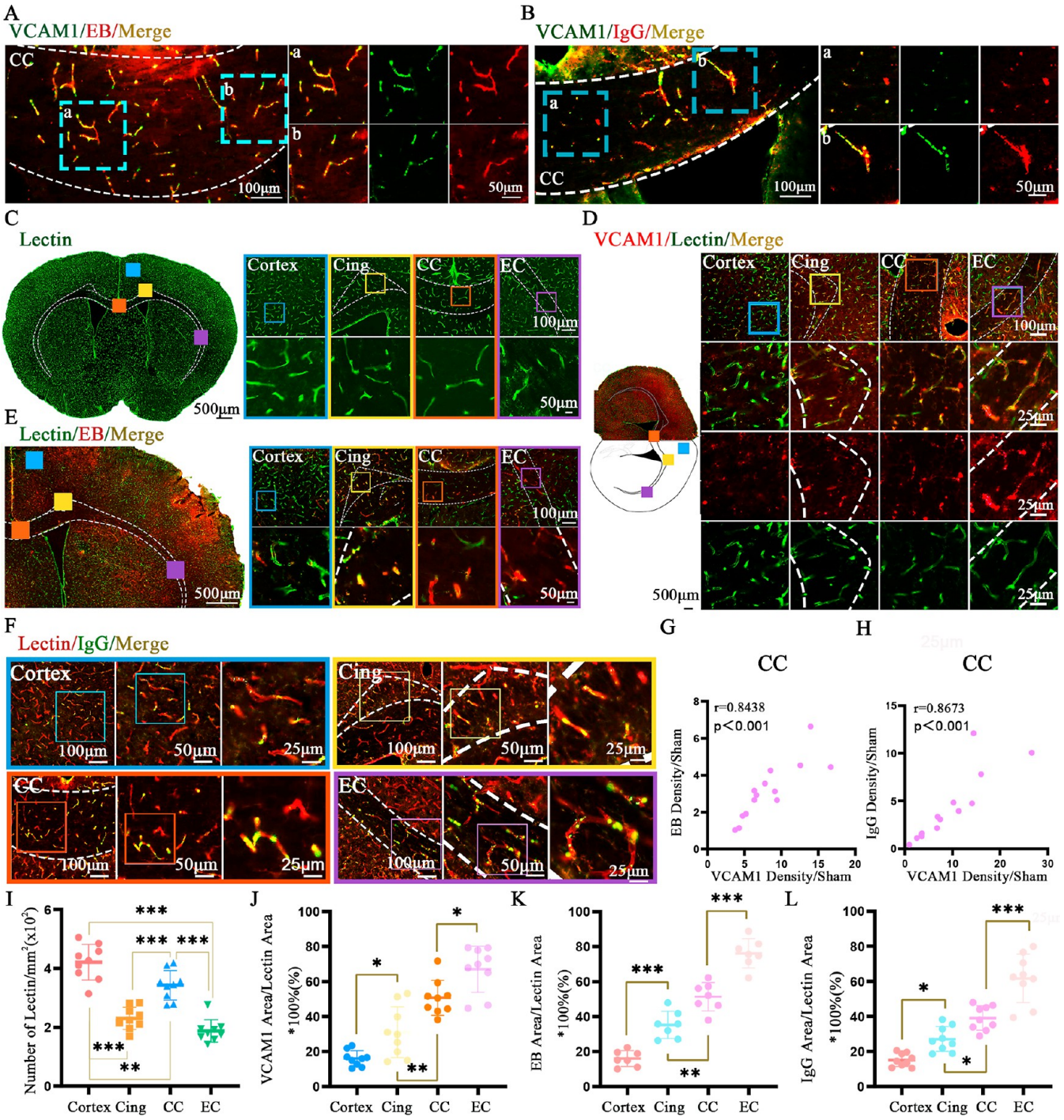

Figure 3. BBB impairment directly correlates with upregulation of VCAM1 on ECs. (A,G) Immunofluorescence staining and quantification of EB and VCAM1 to evaluate the correlation between VCAM1 expression and EB leakage in the CC 3 days post-surgery (VCAM1, green; EB, red; and the region within the white dashed box is CC; $n = 14$). (B,H) Immunofluorescence staining and quantification of IgG and VCAM1 to evaluate the correlation between VCAM1 expression and IgG brain accumulation in the CC 3 days post-surgery (VCAM1, green; IgG, red; and the region within the white dashed box is CC; $n = 13$). (C,I) Immunofluorescence staining and quantification of the blood vessels in four brain areas; blood vessels were labeled by lectin (lectin, green; $n = 9$), (C) left: region in the white dashed box is the white matter. (D,J) Immunofluorescence staining and quantification of VCAM1 in four brain regions 3 days post-surgery; blood vessels were labeled by lectin (VCAM1, red; lectin, green; $n = 9$), (D) left: region in the white dashed box is the white matter. (E,K) Immunofluorescence staining and quantification of EB leakage in four brain areas 3 days post-surgery; blood vessels were labeled by lectin (lectin, green; EB, red; $n = 7$). (E) left: region in the white dashed box is the white matter. (F,L) Immunofluorescence staining and quantification of IgG accumulation in four brain areas 3 days post-surgery; blood vessels were labeled by lectin (lectin, red; IgG, green; $n = 9$); four brain areas include the cortex (blue box), cingulate gyrus (Cing, yellow), corpus callosum (CC, orange), and external capsule (EC, purple). Scales are shown in the figure; ns, not significant; *$p < 0.05$, **$p < 0.01$, and ***$p < 0.001$ compared to the sham group; one-way ANOVA, followed by Dunnett's post hoc test.

https://doi.org/10.1021/acschemneuro.4c00039
ACS Chem. Neurosci. 2024, 15, 2028−2041

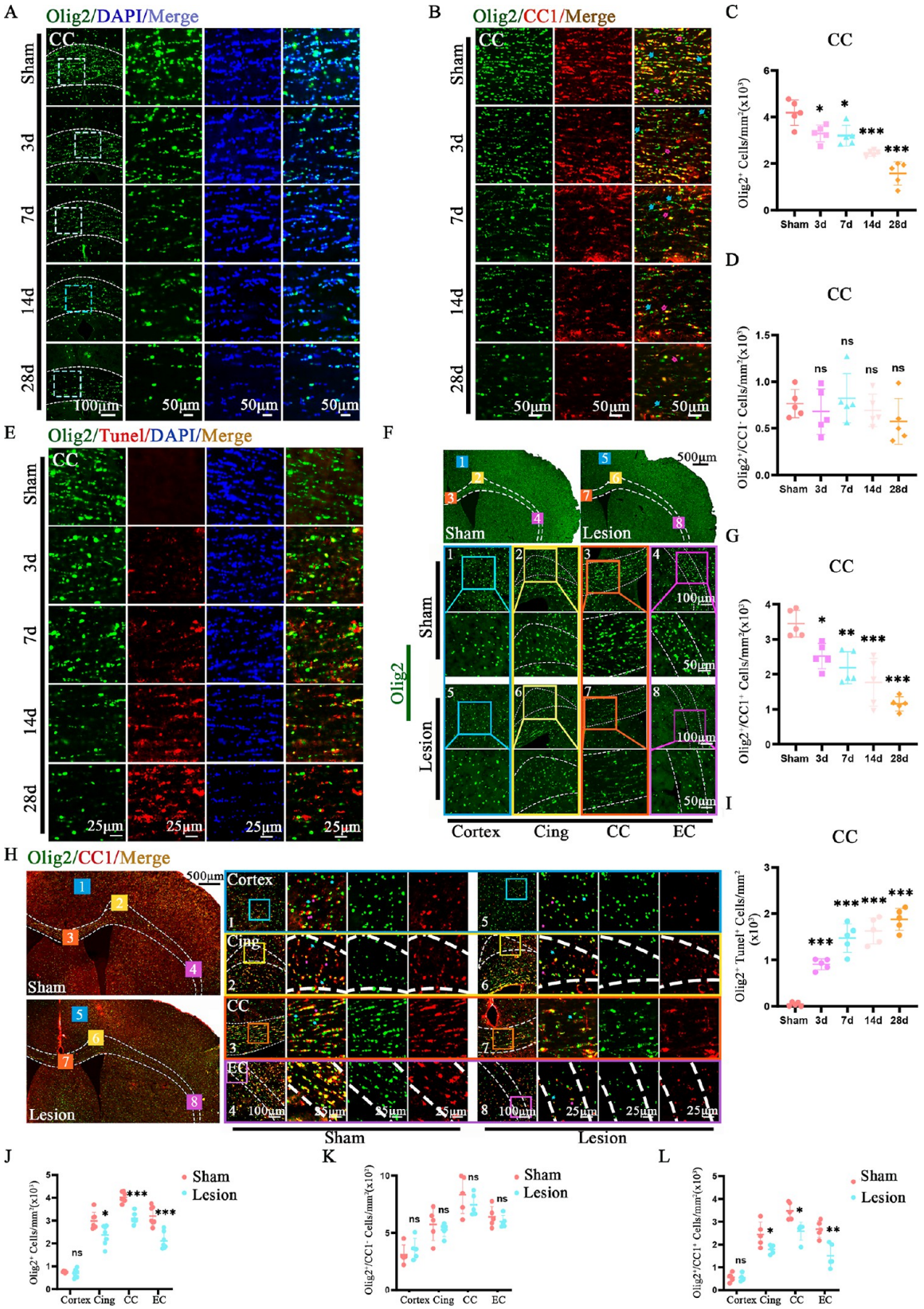

Figure 4. Increased expression of VCAM1 corresponds to different regions of the white matter. (A,C) Immunofluorescence staining and quantification of oligodendrocytes in the CC at different time points after CCH (Olig2, green; $n = 5$). (B) Immunofluorescence staining of Olig2 and CC1 to assess oligodendrocyte alterations in the CC at different time points after CCH (Olig2, green; CC1, red). (D) Quantification of OPCs in the CC at different time points after CCH ($Olig2^+$ and $CC1^-$; $n = 5$). (E) Triple staining for Olig2, terminal deoxynucleotidyl transferase dUTP nick end labeling (TUNEL), and DAPI to evaluate changes in the apoptotic oligodendrocyte number in the CC at different times after CCH (Olig2, green; TUNEL, red; and DAPI, blue). (F,J) Immunofluorescence staining and quantification of oligodendrocytes in four brain areas of the sham group and lesion group (Olig2, green; $n = 7$). In (F), the upper portion depicts the fluorescence staining images of the sham and lesion

https://doi.org/10.1021/acschemneuro.4c00039
ACS Chem. Neurosci. 2024, 15, 2028−2041

Figure 4. continued

groups, while the lower portion shows the stained images of the four brain regions in both groups. Specifically, region 1 represents the cortex in the sham group, region 2 is the Cing in the sham group, region 3 is the CC in the sham group, region 4 is the EC in the sham group, region 5 corresponds to the cortex in the lesion group, region 6 is the Cing in the lesion group, region 7 represents the CC in the lesion group, and region 8 corresponds to the EC in the lesion group. (G) Quantification of mature oligodendrocytes in the CC at different time points after CCH ($Olig2^+$ and $CC1^+$; $n = 5$). (H,K,L) Immunofluorescence staining and quantification of OPCs [(H,K) $Olig2^+$ and $CC1^-$] and mature oligodendrocytes [(H,L) $Olig2^+$ and $CC1^+$] in four brain areas of the sham and lesion groups (Olig2, green; CC1, red; $n = 5$). Left part of (H): the region in the white virtual box is the white matter. In the sham group, region 1 represents the cortex, region 2 corresponds to the Cing, region 3 to the CC, and region 4 to the EC. In the lesion group, region 5 represents the cortex, region 6 corresponds to the Cing, region 7 to the CC, and region 8 to the EC. (I) Quantification of apoptotic oligodendrocytes in the CC at different time points after CCH ($Olig2^+$ and $TUNEL^+$; $n = 5$). Scales are shown in the figure. ns, not significant; $*p < 0.05$, $**p < 0.01$, and $***p < 0.001$ compared to the sham group. One-way ANOVA, followed by Dunnett's post hoc test.

environment.[1−3] Prior studies indicate a strong association between CCH and BBB dysfunction in VD.[11] The dynamic alterations in BBB integrity and cascade reaction that occur following CCH remain largely unclear. We initiated our investigation by assessing the alteration in BBB permeability following CCH. Increased brain water content indicates increased BBB permeability.[17−19] Therefore, we first assessed the changes in brain water content at each time point following CCH. We found that brain water content increased 1 day after CCH, with the most severe brain edema occurring 3 days after CCH (Figure 2B,C). Recovery commenced 7 days after CCH, and brain water content nearly restored to the normal level 28 days after CCH compared to the sham (Figure 2C). To evaluate the temporal profile of BBB permeability changes, we injected Evans Blue (EB) via the tail vein (Figure 2A) and quantified the amount of EB in the white matter through colorimetric analyses at different time points following CCH. As expected, EB accumulated in the brain parenchyma following CCH. EB leakage significantly increased at 3 days post-surgery compared to the sham group. The increase remained significant 7 days post-surgery. However, EB leakage returned to the sham mice level 14 days post-surgery (Figure 2B,D). Furthermore, we simultaneously observed the brain water content and EB content in the control group without CCH and the sham surgery. The results showed that, compared to the control group, there were no significant changes in the brain water content and EB content in the sham surgery group (Figure 2B−D). Then, immune fluorescence staining was employed to further evaluate EB accumulation in the corresponding white matter area following CCH. In the CC, EB fluorescence intensity peaked at 3 days post-surgery and gradually decreased from 7 to 28 days post-surgery (Figure 2E,F). Conversely, the tracer was undetectable in the brain parenchyma region of the sham group (Figure 2E,F). Owing to the increased permeability of the BBB, a fundamental change occurs in the neuropathic interface; that is, the plasma proteins flow into the CNS.[20] As such, plasma immunoglobulin G (IgG) has been extensively used as a reliable marker of BBB disruption in human tissues and relevant animal models.[21] We next examined whether the expression of IgG altered after CCH. Consistently, immunostaining revealed abundant deposition of the plasma-derived IgG outside vessels in the CC following CCH (Figure 2G). The fluorescence intensity of IgG was highest at 3 days post-surgery, which gradually decreased from 7 days to 28 days post-surgery (Figure 2H). The results demonstrated that BBB leakage occurred as early as 1 day after CCH, most severe at 3 days, followed by spontaneous recovery from 7 to 28 days post-surgery. Similar findings were observed in other white matter regions (Figure S2).

2.3. BBB Impairment Directly Correlates with Upregulation of VCAM1 on ECs. We observed a similarity between the trend of BBB permeability changes and VCAM1 expression changes after CCH, with the peak expression of VCAM1 preceding the peak of BBB leakage (Figure 1A,B). This observation suggests that BBB dysfunction may be associated with the upregulation of VCAM1. To further explore their relationship, we quantified the VCAM1 intensity and EB leakage, as well as IgG accumulation in the same brain area. Overall, we observed a positive correlation between the expression of VCAM1 and the severity of EB deposition (Figure 3A), as well as IgG accumulation in the CC (Figure 3B). Furthermore, a significant positive correlation was observed among VCAM1 expression, EB leakage, and IgG accumulation (Figure 3G,H). These data suggest that VCAM1 may be a potent permeability factor for BBB dysfunction after CCH. To confirm this conclusion, we further compared VCAM1 density and BBB leakage in various brain regions after CCH. We investigated the correspondence between the distribution patterns of VCAM1 expression and BBB leakage. Initially, we compared VCAM1 expression on microvasculars in each brain region after CCH. We selected the time point of 3 days post-surgery and quantified the VCAM1 expression of four brain regions, including the cortex, CC, Cing, and EC. To except for differences in blood vessel density among brain regions (Figure 3C,I), we used the VCAM1 area/lectin area index to evaluate VCAM1 expression in each region. The highest expression of VCAM1 was observed in EC, followed by the CC, Cing, and finally the cortex (Figure 3D,J). This finding suggests that different brain regions have different sensitivity to ischemic. Subsequently, we examined if similar variations in BBB permeability existed across different brain regions. We observed that EB leakage was more pronounced in the white matter compared to the cortex, with the EC exhibiting the most substantial leakage, followed by the CC and then the Cing (Figure 3E,K). The results of IgG immunofluorescence staining were consistent (Figure 3F,L). This observation suggests that the BBB leakage is more pronounced in the white matter than in the cortex, with the EC experiencing the most severe injury following CCH. It is noteworthy that the areas with higher expression of VCAM1 showed more severe BBB leakage. This finding suggests varying degrees of inflammatory activation across different brain regions following CCH, consistent with the distribution patterns of BBB leakage. Additionally, this correlation suggests that endothelial inflammation is a significant factor contributing to BBB leakage following CCH.

https://doi.org/10.1021/acschemneuro.4c00039
ACS Chem. Neurosci. 2024, 15, 2028−2041

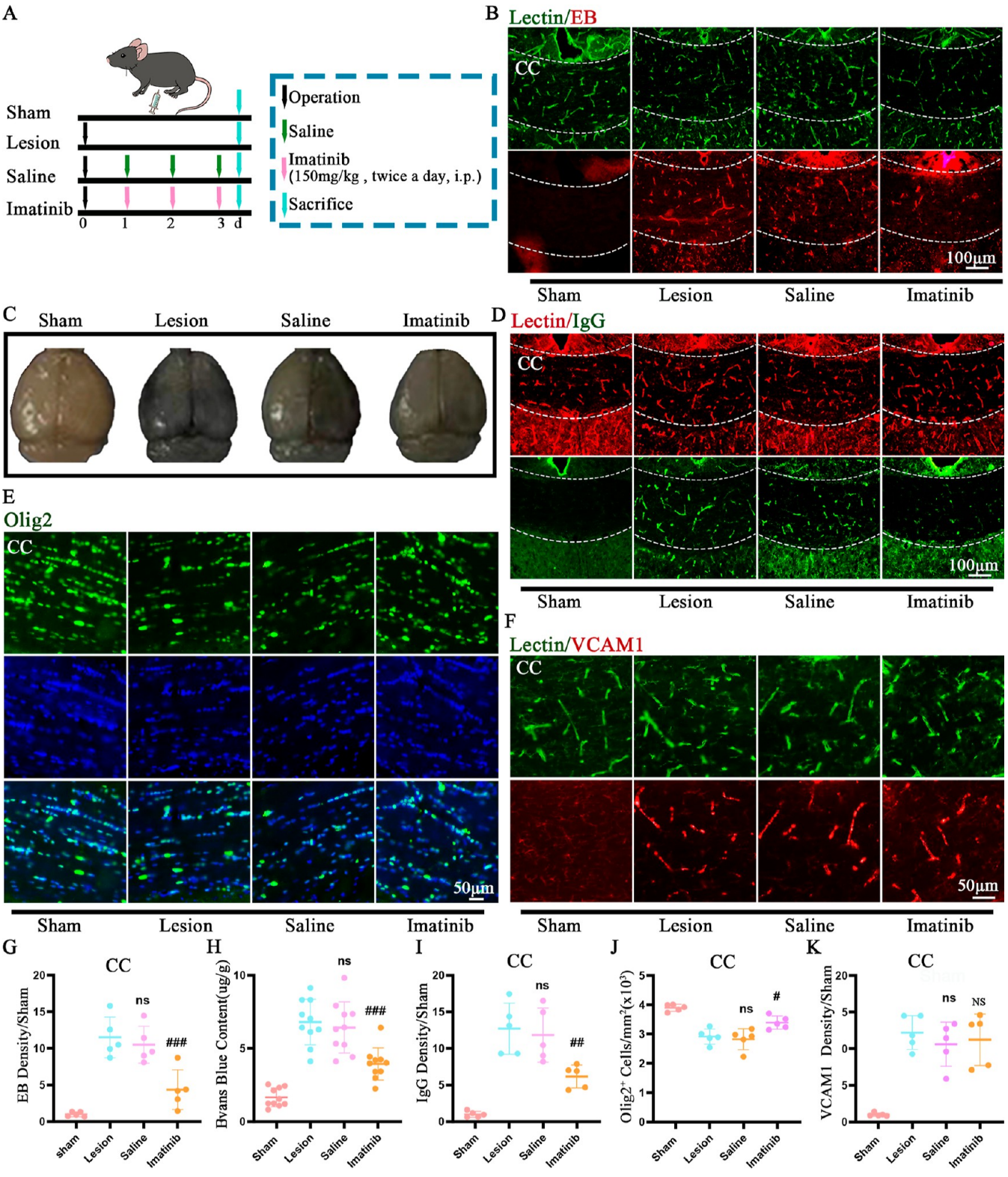

Figure 5. Imatinib effectively protected both the BBB and the brain parenchyma following CCH. (A) Schematic illustration of the imatinib treatment procedures. (B,G) Immunofluorescence staining and quantification of EB leakage following imatinib treatment in the CC; blood vessels were labeled by lectin (lectin, green; EB, red; and the region within the white dashed box is CC; $n = 5$). (C,H) Representative EB images and quantification of the EB content ($n = 10$). (D,I) Immunofluorescence staining and quantification of IgG brain accumulation following imatinib treatment in the CC; blood vessels were labeled by lectin (lectin, red; IgG, green; and the region within the white dashed box is CC; $n = 5$). (E,J) Immunofluorescence staining and quantification of oligodendrocytes in the CC (Olig2, green; DAPI, blue; $n = 5$). (F,K) Immunofluorescence staining and quantification of VCAM1 expression following imatinib treatment in the CC; blood vessels were labeled by lectin (lectin, green; VCAM1, red; $n = 5$). Scales are included in the figure. ns, not significant compared to the lesion group; NS, not significant; $^{\#}p < 0.05$, $^{\#\#}p < 0.01$, and $^{\#\#\#}p < 0.001$ compared to the saline group. One-way ANOVA, followed by Dunnett's post hoc test.

https://doi.org/10.1021/acschemneuro.4c00039
ACS Chem. Neurosci. 2024, 15, 2028−2041

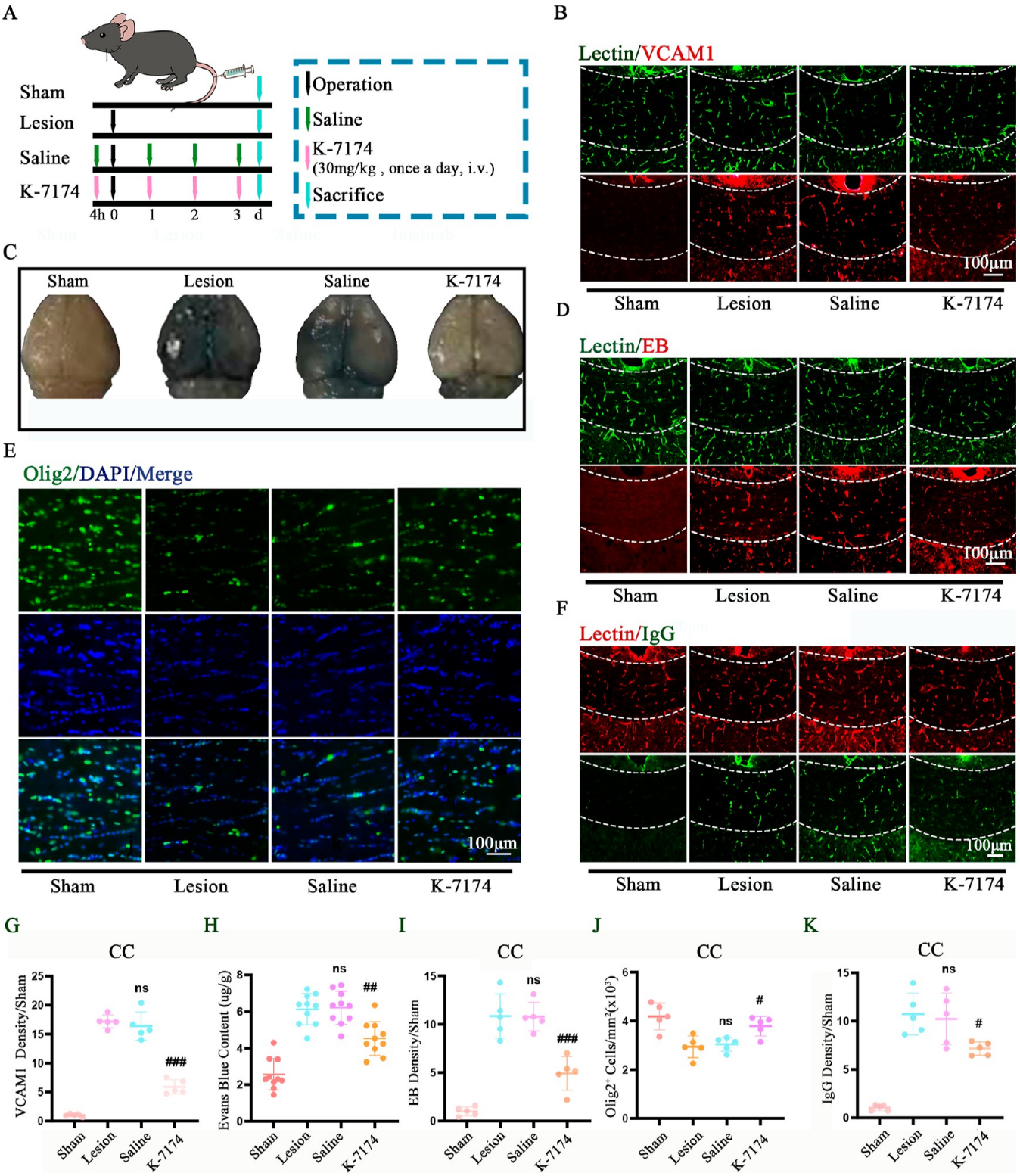

Figure 6. Extravasation of EB and IgG and loss of oligodendroglias is improved following VCAM1 inhibitor (K-7174) treatment. (A) Schematic illustration of the procedures for VCAM1 inhibitor treatment. (B,G) Immunofluorescence staining and quantification of VCAM1 following VCAM1 inhibitor treatment in the CC; blood vessels were labeled by lectin (lectin, green; VCAM1, red; and the region within the white dashed box is CC; $n = 5$). (C,H) Representative images depicting EB distribution and quantification of EB content following VCAM1 inhibitor treatment ($n = 10$). (D,I) Immunofluorescence staining and quantification of EB leakage following VCAM1 inhibitor treatment in the CC; blood vessels were labeled by lectin (lectin, green; EB, red; and the region within the white dashed box is CC; $n = 5$). (E,J) Immunofluorescence staining and quantification of oligodendrocytes following VCAM1 inhibitor treatment in the CC (Olig2, green; DAPI, blue; $n = 5$). (F,K) Immunofluorescence staining and quantification of IgG brain accumulation following VCAM1 inhibitor treatment in the CC; blood vessels were labeled by lectin (lectin, red; IgG, green; and the region within the white dashed box is CC; $n = 5$). Scales are provided in the figure. ns, not significant compared to the lesion group; $^{\#}p < 0.05$, $^{\#\#}p < 0.01$, and $^{\#\#\#}p < 0.001$ compared to the saline group. One-way ANOVA, followed by Dunnett's post hoc test.

https://doi.org/10.1021/acschemneuro.4c00039
ACS Chem. Neurosci. 2024, 15, 2028−2041

2.4. Increased Expression of VCAM1 Corresponds to Different Regions of the White Matter. Previous studies have demonstrated that WMLs, resulting from BBB leakage following CCH, represent another fundamental pathological alteration in VD.[5,18] To explore the potential association between WMLs and the upregulation of VCAM1 in microvessels, we initially examined the pathological alterations in the white matter at different time points following CCH. The white matter comprises nerve fibers and abundant glial cells. Normal and stable glial function is crucial for maintaining the white matter integrity and function.[22] Oligodendrocytes comprise approximately 40% of glia cells, and oligodendrocyte precursor cells (OPCs) undergo two additional stages of differentiation to become into immature oligodendrocytes. Subsequently, oligodendrocytes mature progressively, and mature oligodendrocytes can synthesize sphingomyelin, which is the crucial component of the axonal myelin sheath of neurons. The integrity of the myelin sheath is the fundamental for functioning of axonal signaling.[23] Since WMLs result from the loss of mature myelin-producing oligodendrocytes, we initially examined the changes in oligodendrocytes in the CC following CCH. Staining for Olig2 in the CC of 3 day group, compared to the sham group, revealed an approximately 25% decrease in oligodendrocyte density, which worsened with prolonged ischemia time (Figure 4A,C). Immunostaining of oligodendrocytes in the CC revealed no alteration in the numbers of OPCs with Olig2 positivity and CC1 negativity at 3 days post-surgery compared to the sham group (Figure 4B,D). However, the number of mature oligodendrocytes, showing both Olig2 and CC1 positivity, was significantly reduced compared to the sham group, and this reduction exacerbated with prolonged ischemia time (Figure 4B,G). Oligodendrocyte apoptosis was observed in the CC at 3 days post-surgery (Figure 4E,I). Comparable findings were also documented in other white matter regions (Figure S3). Myelin basic protein (MBP) serves as a marker of the myelin sheath surrounding neuronal axons.[24] Immunofluorescence staining showed a gradual decrease in the density of MBP in each white matter region from 14 to 28 days following CCH (Figure S4A,C−E). Thus, it was suggested that demyelination occurred in the white matter following CCH. Neurofilament (NF) is regarded as a useful indicator for estimating axonal degeneration.[25] Staining results of NF revealed that axonal injury initiates 28 days post-surgery in the white matter (Figure S4B,F−H). These results suggest that WMLs began to occur from 3 days post-surgery and worsened with time, with the upregulation of VCAM1 preceding the formation of WMLs (Figure 1A,B), indicating a potential association between increased VCAM1 expression and WMLs. Subsequently, we compared the extent of pathological damage in various brain regions to further explore the correlation between brain endothelial inflammation and brain parenchymal lesions. Immunofluorescence staining results revealed that the density of oligodendrocytes decreased by approximately 33% in the EC, 25% in the CC, and 20% in the Cing in the 3 day group compared to the sham group. No changes were noted in the cortex (Figure 4F,J). Previous results have indicated that the disruption of oligodendrocyte lineage homeostasis after CCH was primarily due to the loss of mature oligodendrocytes. Therefore, we further compared the changes in the number of mature oligodendrocytes in four brain regions. As anticipated, the greatest proportion of mature oligodendrocytes in the EC was lost. The density of mature oligodendrocyte decreased by 41% in the EC, 31% in the CC, and 25% in the Cing at 3 days post-surgery (Figure 4H,K,L). This finding suggests that the pathological damage to the EC was the most severe after CCH, consistent with the regional variations in endothelial inflammation and BBB impairment (Figure 3D−F,J−L). Collectively, these results suggest that VCAM1-driven endothelial inflammation may be the crucial pathological mechanism underlying WMLs following CCH.

2.5. Enhancing BBB Permeability Does Not Influence Endothelial Inflammation Following CCH. Previous results have revealed a robust association between endothelial inflammation and BBB injury. However, it remains unclear whether VCAM1-driven endothelial inflammation is the primary cause of BBB breakdown following CCH or a secondary consequence of this damage. Hence, we employed imatinib to further investigate the causal relationship between them. Imatinib can effectively reduce BBB permeability by inhibiting the signaling of platelet-derived growth factor receptor alpha (PDGFR-α) in ischemic stroke.[26] Initially, we evaluated the impact of imatinib treatment on the BBB integrity and neural function following CCH. We also investigated whether the decreased BBB permeability affects endothelial inflammation after CCH. Since BBB leakage was most pronounced at 3 days post-surgery (Figure 2B−H), we chose 3 days post-surgery as the observation point. We observed that imatinib treatment significantly decreased the EB leakage and IgG accumulation compared to the saline group in the CC (Figure 5B−D,G−I). This finding suggests that imatinib effectively preserves the BBB integrity following CCH. We further evaluated the pathological outcomes following imatinib treatment and observed an increase in the number of oligodendroglias compared to the saline group in the CC (Figure 5E,J). However, VCAM1 levels did not show significant changes after imatinib treatment (Figure 5F,K). These findings indicate that decreased BBB permeability confers protective effects on the brain parenchyma but does not influence endothelial inflammation.

2.6. Inhibition of VCAM1 Activation Mitigates BBB Impairment and Brain Parenchyma Injury. Prior research has shown that inhibiting the VCAM1 expression can mitigate the inflammatory responses and decrease the infiltration of circulating immune cells into the brain parenchyma.[19] We assessed the impact of treatment with the VCAM1 inhibitor (K-7174) on the inflammatory response and its protective effects on the BBB and brain parenchyma following CCH. We examined the effects of BCAS on the brain at various time points post-surgery and noted that vascular leakage and BBB dysfunction were most pronounced at 3 days post-surgery (Figure 2B−H). Therefore, we selected 3 days post-surgery to observe the effects of VCAM1 inhibitor on the BBB, and we verified the blockade of VCAM1 activation by VCAM1 inhibitors and observed reduced VCAM1 expression in the K-7174 group compared to the saline group (Figure 6B,G). To assess whether the VCAM1 inhibitor can alleviate BBB leakage in vivo, a BBB permeability test was conducted in mice injected with the VCAM1 inhibitor via the tail vein. A substantial leakage of EB and IgG was observed in the CC at 3 days after CCH (Figure 2B−H). However, treatment with the VCAM1 inhibitor significantly attenuated the extravasation of EB and IgG in the CC (Figure 6C,D,F,H,I,K), indicating that the VCAM1 inhibitor preserved BBB integrity. Furthermore, we evaluated the pathological outcomes following VCAM1 inhibitor treatment and observed an increased number of

https://doi.org/10.1021/acschemneuro.4c00039
ACS Chem. Neurosci. 2024, 15, 2028−2041

oligodendrocytes in K-7174 group compared to the saline group (Figure 6E,J). Similar alterations were noted in the Cing and EC (Figure S5). Our previous findings indicated that demyelination occurred 14 days after CCH, and axonal injury was observed 28 days after CCH compared to the sham group. Therefore, in order to further validate the effects of K-7174 on the pathological phenotype, we prolonged the duration of K-7174 injection to 28 days post-surgery and observed a reduction in white matter demyelination and axonal injury in the K-7174 group compared to the saline group (Figure S6). These findings suggest that the VCAM1 inhibitor effectively reduces endothelial inflammation in brain microvessels following CCH, thereby potentially improving BBB and reducing brain injury. This observation further supports the association between BBB dysfunction and WMLs with endothelial inflammation after CCH.

3. DISCUSSION

VD is becoming a major public health concern worldwide.[27] Considerable evidence indicates a link between CCH and VD,[28] although the causal relationship remains unclear. CCH triggers a cascade of molecular and cellular responses leading to BBB breakdown and neurodegeneration.[29] BBB dysfunction and WMLs associated with CCH are fundamental pathological alterations in VD. While CCH, BBB dysfunction, and WMLs are recognized as common pathophysiologial features in VD, the molecular mechanisms underlying BBB breakdown and WMLs following CCH have not yet been properly examined. In this study, we investigated the temporal progression of BBB dysfunction and WMLs following CCH. We found that the BBB leakage precedes other pathological events, such as mature oligodendrocyte loss, white matter demyelination, and axonal damage following CCH. Additionally, we conducted a comprehensive assessment of VCAM1 expression on microvessels at various postoperative time points. Our findings indicate that CCH upregulates VCAM1 expression on ECs, resulting in increased BBB permeability and brain parenchymal injury. Furthermore, treatment with the VCAM1 inhibitor alleviated BBB impairment and brain parenchyma injury following CCH.

Collectively, these findings indicate that endothelial inflammation predominantly regulates the occurrence of increased BBB permeability and WMLs following CCH, suggesting that endothelial inflammation is the primary diver of BBB impairment and progressive neural dysfunction. Targeting endothelial inflammation reversal may represent a promising therapeutic strategy for VD. The BBB restricts the free diffusion of molecules from the blood into the brain parenchymal to maintain brain microenvironment homeostasis.[30] The BBB impairment and WMLs are two primary pathological hallmarks in VD. BBB dysfunction contributes to the pathology of numerous neurological conditions, such as stroke,[31] Alzheimer's disease (AD),[32] aging[33] and cerebral small vessel disease (CSVD).[6] Recent studies have shown that BBB dysfunction in the hippocampus precedes cognitive impairment in AD.[34] BBB dysfunction serves as an early biomarker of AD.[34] Furthermore, in normal aging, white matter integrity remains intact despite BBB impairment.[35] Moreover, our study revealed that CCH is linked to transient yet severe BBB impairment. Severe BBB leakage was evident as early as 1 day following CCH, peaked at 3 days, and spontaneously resolved between 7 days and 28 days post-surgery. BBB breakdown precedes the development of WMLs, characterized by notable oligodendrocyte lineage apoptosis, demyelination, and axonal degeneration. Moreover, reducing BBB permeability effectively ameliorates WMLs. In summary, previous research and our findings indicate that BBB dysfunction occurs early in the course of neurological diseases, with BBB impairment serving as a primary contributor to brain parenchymal injury.

BBB dysfunction serves as the link between blood-derived pathogens and neural dysfunction. Cellular constituents of the BBB encompass ECs, pericyte, and other components. ECs play a crucial role in facilitating direct communication between the blood and the brain parenchyma. EC function is essential for preserving BBB integrity. Research has indicated that EC dysfunction primarily underlies BBB dysfunction in stroke-prone spontaneously hypertensive rats.[36] This rat model serves as a model for human sporadic CSVD,[37] suggesting that EC dysfunction is a significant contributor to BBB impairment. Endothelial inflammation is one of the typical pathological changes of endothelial dysfunction. To investigate whether VCAM1-driven endothelial inflammation triggers BBB breakdown and WML formation after CCH, we selected white matter as the focus of our investigation. WMLs represent a characteristic pathological feature of VD.[11] In recent years, there has been growing recognition of the importance of white matter in cognition, as white matter tracts form an integral component of complex neural networks supporting various neurobehavioral functions.[38] However, clinical observations indicate that different types of dementia exhibit distinct patterns of involvement. For instance, patients with cerebral autosomal dominant arteriopathy with subcortical infarcts and leukoencephalopathy (CADASIL) typically exhibit WMLs in the temporal pole and the external capsule.[39] Likewise, patients with AD commonly present with WMLs in the parietal lobe.[40] Conversely, patients with vascular cognitive impairment typically exhibit changes in all regions of white matter except the occipital lobe.[41] Certain researchers posit that the extent of cognitive impairment resulting from WMLs depends on factors such as their location, volume, and patients' cognitive reserve.[42] The location of cognitive impairment may be affected primarily by the location of WMLs.[43] Thus, we divided the white matter into three regions—the CC, EC, and Cing, to comprehensively examine the dynamic changes occurring throughout the brain following CCH. Our findings suggest that VCAM1-driven endothelial inflammation may primarily contribute to BBB impairment, with other pathological changes potentially secondary to endothelial inflammation following CCH. First, we noted a strong positive correlation between the VCAM1 expression and BBB permeability. Regions exhibiting significant VCAM1 expression demonstrated severe BBB leakage, whereas those with low VCAM1 protein levels showed less pronounced BBB leakage. These findings together imply that VCAM1 may be a potent endothelial permeability factor. Second, the peak expression of VCAM1 on ECs precedes the peaks of BBB leakage and WML formation. Significant expression of VCAM1 on the microvessels was observed at 1 day post-surgery, that is, at the early stage of CCH. The expression of VCAM1 protein gradually decreased from 3 to 28 days post-surgery. Nevertheless, the peak of BBB leakage was observed at 3 days post-surgery. Our findings demonstrated that EB leakage and IgG brain accumulation were most pronounced at 3 days post-surgery. The majority of the pathological changes in the brain parenchyma occurred primarily after 3 days post-surgery.

https://doi.org/10.1021/acschemneuro.4c00039
ACS Chem. Neurosci. 2024, 15, 2028−2041

Significant loss of mature oligodendrocytes in the white matter occurred 3 days post-surgery, leading to apoptosis of oligodendroglial lineage cells and disrupted homeostasis, ultimately resulting in irreversible WMLs. Moreover, demyelination of the white matter was observed up to 14 days post-surgery, with axonal injury noted at 28 days post-surgery, which resulted in neurological degeneration. While VCAM1 upregulation on microvascular is a transient process and can spontaneously recover following CCH, VCAM1-induced brain parenchymal injury persists. Third, various brain regions exhibit different sensitivity to ischemia, leading to varying degrees of endothelial inflammation, BBB leakage, and brain parenchymal injury. Nonetheless, the distribution pattern remained consistent, with brain regions exhibiting severe endothelial inflammation also demonstrating more pronounced BBB leakage and brain parenchymal damage. Remarkably, the white matter exhibited greater sensitivity to ischemia compared to the cortex, consistent with the significant WMLs in VD. White matter vascular changes were most prominent in VD.[44] This heightened sensitivity of the white matter to hypoperfusion is attributed to their reliance on the centripetal long medullary artery and centrifugal anterior choroidal artery or bean artery, with limited anastomoses and watershed blood-supply areas. Finally, intraperitoneal injection of imatinib, known for its efficacy in BBB protection following CCH,[18,26] reduced BBB permeability and ameliorated various pathological events, albeit without affecting VCAM1 expression of brain microvessels. In conclusion, VCAM1 upregulation emerges as a pivotal pathophysiological mechanism underlying BBB impairment and WMLs in VD, underscoring its significant implications for the development of novel therapeutic strategies in VD. Consequently, we administered the VCAM1 inhibitor via the tail vein, which led to significantly reduced VCAM1 activation compared to the saline group, resulting in notable improvement in BBB leakage and WMLs following CCH. This discovery underscores the critical role of VCAM1 in the progression of VD. Sensitive endothelial inflammation response in the white matter following CCH may contribute to the white matter's susceptibility to injury. Therefore, drugs targeting VCAM1 could be useful for the early intervention of neurological diseases. While our findings indicate VCAM1's involvement in the overall regulation of BBB dysfunction after CCH, the specific pathological cascade linking them remains unclear. Thus, additional neuropathological studies are necessary to elucidate this crucial aspect of BBB dysfunction and brain endothelial inflammation.

4. CONCLUSIONS

In summary, our findings implied that VCAM1 regulates BBB permeability and the formation of WMLs following CCH. We found that VCAM1 upregulation results in BBB dysfunction, initiating a cascade of pathological events, including mature oligodendrocyte death and WML formation. The inhibition of VCAM1 effectively protected both the BBB and the brain parenchyma. Thus, our findings have important implications for understanding the pathogenesis of VD and suggest that VCAM1 upregulation is a key trigger point. Based on these insights, potential therapeutic strategies for VD can be developed.

5. MATERIALS AND METHODS

5.1. Animals. Adult male C57BL/6J mice (weight: 25−30 g and age: 9−12 weeks) selected for this study were housed at a temperature of 24−26 °C on a 12 h light/dark cycle with free access to food and water. All experimental procedures were approved by the National Institutes of Health guide for the care and use of Laboratory animals. Every effort was made to minimize the number of animals and their suffering. In the quantitative analysis of brain water content and EB at different time points after CCH, mice were divided into the control group, sham group, 1 day group, 3 day group, 7 day group, 14 day group, and 28 day group following CCH. In the experiment of observing different time points after CCH, mice were randomly assigned to the sham group, 1 day group, 3 day group, 7 day group, 14 day group, and 28 day group. In the imatinib treatment experiment, mice were randomly assigned into the sham group, lesion group, saline group, and imatinib group. In the K-7174 treatment experiment, mice were randomly assigned into the sham group, lesion group, saline group, and K-7174 group. All sham group mice present in this experiment were mice 3 days after sham surgery; we evaluated BBB dysfunction and VCAM1 expression in CC at 1, 3, 7, 14, and 28 days post-sham surgery. First, we compared the expression levels of VCAM1 in the CC at different time points following sham surgery. As anticipated, there were no significant differences observed among the groups of mice (Figure S7A,E). Subsequently, we assessed BBB integrity by measuring dye leakage following the injection of EB into the tail vein. Consistently, there were no significant differences in EB content in the CC at various time points post-sham surgery (Figure S7B,F). Immunofluorescence staining was employed to corroborate these findings and assess EB accumulation in the CC at various time points post-sham surgery. The fluorescence intensity of EB did not differ significantly among the groups (Figure S7C,G). Following BBB breakdown, endogenous circulating macromolecules leak into the brain.[45] Immunostaining showed no significant variation in IgG accumulation in the CC among the groups (Figure S7D,H). These findings indicate that sham-operated mice showed no changes in BBB permeability or VCAM1 expression at 1−28 days post-sham surgery. Information regarding the number of mice used for each specific experiment can be found in the figure legends. Treatment was administered in a blind manner.

5.2. Establishment of the CCH Model. The BCAS model was prepared as described previously.[46] The micro-coil specifications used are as follows: NITI material, inner diameter 0.18 mm, wire diameter 0.08 mm, length 2.5 mm, and intercept 0.5 mm (purchased from SAMINI SPRING CO, Ltd.). The experimental mice were anesthetized by 1−1.5% isoflurane/air. Body temperature (36.5 °C ± 0.5 °C) was monitored during the experiments using an abdominal pressure-sensitive probe and a rectal temperature probe. The isoflurane dose and heated airflow were adjusted continuously to ensure stable and reproducible depth of anesthesia. A longitudinal incision of approximately 1 cm was made in the middle of the mouse's neck. Then, the common carotid artery (CCA) was exposed by an operation of the bilateral carotid sheath. The mice in the sham group were sutured after this operation. The mice in the BCAS group were twinned by a microcoil around their CCA. The entire surgery was performed by placing the mice on a heating pad, with the rectal temperature maintained at 36.5−37 °C. The mice were observed and cared postoperatively until their consciousness was recovered, with free access to food and water.

5.3. Measurement of Brain Water Content. The mice were anesthetized and perfused intracardially with cold 0.9% saline. Next, the brains were removed, and the brainstem and cerebellum were removed. To measure brain water content, the brains was weighed before and after being dehydrated in an oven for 24 h at 100 °C. The wet/dry brain weight ratio was used to quantify brain water content for statistical analysis.

5.4. EB Extravasation. EB extravasation was performed to assess the BBB permeability.[47] Briefly, 2% EB (2 mL/kg, Sigma-Aldrich) was injected via the tail vein at various time points, as indicated. The EB was allowed to circulate in the mice for 30 min. At the end of the 30

https://doi.org/10.1021/acschemneuro.4c00039
ACS Chem. Neurosci. 2024, 15, 2028−2041

min, the mice were euthanized with carbon dioxide. Cardiac perfusion of 20 mL 1× PBS was performed to remove the residual EB in the blood, after which the brain was harvested and stored in dry ice. The brain tissues were weighed, and approximately 50% of the trichloroacetic acid (TCA) solution (diluted in 0.9% saline) was calculated based on a 1:2 ratio of weight (mg)/volume (μL). The tissue was homogenized in the TCA solution. The mixture was then sonicated (10 cycles, 30 s on, 30 s off). Subsequently, the mixture was allowed to incubate overnight at 4 °C on a rotator to allow for the complete extraction of EB from the brain tissues. The TCA−lysate mixture was then centrifuged (30 min, 15,000 rcf, 4 °C), after which the supernatant was collected. The supernatant was loaded in a 96-well plate with the supplementation of 95% ethanol in a 1:3 ratio, respectively. The plate was then placed into a spectrophotometer at 620 nm to determine the EB concentration.

5.5. Immunofluorescence. The mice were anesthetized and perfused intracardially with cold 4% paraformaldehyde (PFA, pH 7.4), followed by perfusion with PBS. Next, the brains were removed, postfixed overnight, and finally cryoprotected in phosphate-buffered sucrose (30%) for 3−5 days. Immunohistochemistry staining for the frozen sections was performed using a previously described protocol.[48] The following primary antibodies were used in the study: rabbit anti-immunoglobulin G (IgG, 1:200, 315005003, Jackson ImmunoResearch), rabbit anti-Olig2 (1:200, AB9610, Millipore), mouse anti-CC1 (1:200, OP80, Calbiochem), mouse anti-myelin basic protein (1:200, 808401, Biolegend), mouse anti-neurofilament (1:200, 801701, Biolegend), mouse anti-VCAM1 (1:200, 66294-1-Ig, Proteintech), rabbit anti-VCAM1 (1:200, DF6082, Affinity), rabbit anti-CD31 (1:200, GB11063-1-100, Servicebio), Lectin-488 (1:300, DC-1174, Vector Laboratories), and Lectin-594 (1:300, DC-1177, Vector Laboratories); the following secondary antibodies were used in the study: Alexa Fluor 594-conjugated goat anti-rabbit IgG (1:500, A-11012, Invitrogen, USA), Alexa Fluor 594-conjugated goat anti-mouse IgG (1:500, A-11032, Invitrogen, USA), Alexa Fluor 488-conjugated goat anti-rabbit IgG (1:500, A-11034, Invitrogen, USA), and Alexa Fluor 488-conjugated goat anti-mouse IgG (1:500, A-11001, Invitrogen, USA). Nuclear staining was performed using 4′,6′-diamidino-2-phenylindole dihydrochloride (DAPI, 1:2000, Thermo Fisher). All images were visualized by using an Olympus BX53 microscope.

5.6. TUNEL Assay. The TUNEL assay was performed by using the cell death detection kit (Beyotime, C1086, China) according to the manufacturer's instructions. Briefly, the frozen brain tissue slices were fixed for 30−60 min with 4% polymerization, then washed with PBS, and fixed with the buffer provided in the kit. After incubating overnight, the frozen brain tissue slices were washed with PBS. Next, immunohistochemistry staining for the frozen sections was performed using a previously described protocol.[49] DAPI was used to label the cell nuclei for 10 min. Under the fluorescence microscope, the cells with a dark red fluorescence were defined as apoptotic cells.

5.7. Treatment with Imatinib. Imatinib has been found to maintain the BBB integrity.[18] After CCH, the mice were administered imatinib (150 mg/kg) by i.p. injections every 12 h for 3 days. The lesion control mice were administered normal saline after CCH. After the final injection, the mice were euthanized and perfused.

5.8. Treatment with the VCAM1 Inhibitor. VCAM1 plays a critical role in the inflammatory reactions from the original recruitment of leukocytes through successive steps in the continuing process.[50] A potent inhibitor of cell adhesion to endothelial cells, K-7174, was selected. This compound inhibited the VCAM1 expression but not the expression of intercellular cell adhesion molecule 1 or e-selectin expression induced by inflammatory cytokines.[51] K-7174 (30 mg/kg, MCE) was injected through the tail vein of the mouse 4 h before and then every day after the operation. The lesion control mice were administered normal saline after CCH. After the final injection, the mice were euthanized and perfused.

5.9. Cell Counts. To quantify the number of various cell types in the Cing, CC, EC, and cortex, five fields were randomly selected from each section and imaged under a light microscope (BX53, Olympus, Japan) with a 20× or 40× objective in 10−12 μm-thick z-stacks. A total of five sections were analyzed. Every cell expressing the selected marker was manually counted using ImageJ (National Institutes of Health, USA). The data were presented as the average cell number in a single field per section.

5.10. Statistical Analysis. Data normality was assessed using the Shapiro−Wilk test. Comparisons between multiple group comparisons were made by one-way ANOVA, followed by Dunnett's post hoc test or two-way ANOVA. For all unpaired *t* tests, the F test for equality of variance was performed. The data were presented as the mean ± SD. All statistical analyses were performed with GraphPad Prism 8.0 software. The values were considered significant at $p < 0.05$.

■ ASSOCIATED CONTENT

Data Availability Statement

The authors declare that all data supporting the results in this study are available in the paper and its Supporting Information.

Supporting Information

The Supporting Information is available free of charge at https://pubs.acs.org/doi/10.1021/acschemneuro.4c00039.

Immunofluorescence staining images of VCAM1, EB, IgG, and oligodendrocytes in Cing and EC following CCH; alterations in myelination and axons post-CCH, as well as amelioration of Cing and EC by K-7174; and phenotype comparison conducted among sham groups at different time points (PDF)

■ AUTHOR INFORMATION

Corresponding Author

Jiewen Zhang − *Department of Neurology, Zhengzhou University People's Hospital, Henan Provincial People's Hospital, Zhengzhou, Henan 450003, China;* orcid.org/0000-0001-6784-6658; Email: zhangjiewen9900@126.com

Authors

Huiwen Zhang − *Department of Neurology, Zhengzhou University People's Hospital, Henan Provincial People's Hospital, Zhengzhou, Henan 450003, China*

Junkui Shang − *Department of Neurology, Zhengzhou University People's Hospital, Henan Provincial People's Hospital, Zhengzhou, Henan 450003, China*

Wei Li − *Department of Neurology, Zhengzhou University People's Hospital, Henan Provincial People's Hospital, Zhengzhou, Henan 450003, China*

Dandan Gao − *Department of Neurology, Renmin Hospital of Wuhan University, Wuhan, Hubei 430072, China*

Complete contact information is available at: https://pubs.acs.org/10.1021/acschemneuro.4c00039

Author Contributions

H.W.Z. and J.K.S. have contributed equally to this work and share first authorship. J.W.Z. contributed to the conception and design. H.W.Z. performed the literature search and drafted this paper. J.K.S. analyzed the data. W.L. and D.D.G. revised the manuscript.

Funding

This study was supported by the National Natural Science Foundation of China (grants 82171196 and 81873727). Henan Province Medical Science and Technology Research Project (grant LHGJ2019779). Henan Province Key Science and Technology Program, China (201701020).

Notes

The authors declare no competing financial interest.

All animal protocols were approved by the National Institutes of Health guide for the care and use of Laboratory animals. Consent to Participate: not applicable. This research did not involve human subjects.

■ ABBREVIATIONS

AD, Alzheimer's disease; BBB, blood−brain barrier; BCAS, bilateral common carotid artery stenosis; CC, corpus callosum; CCA, common carotid artery; CCH, chronic cerebral hypoperfusion; Cing, cingulated gyrus; CNS, central nervous system; CSVD, cerebral small vessel disease; EB, Evans Blue; EC, external capsule; ECs, endothelial cells; IgG, immunoglobulin G; MBP, myelin basic protein; NF, neurofilament; OPCs, oligodendrocyte precursor cells; TCA, trichloroacetic acid; TUNEL, terminal deoxynucleotidyl transferase dUTP nick end labeling; VCAM1, vascular cell adhesion molecule1; VD, vascular dementia; WMLs, white matter lesions

■ REFERENCES

(1) Montagne, A.; Zhao, Z.; Zlokovic, B. V. Alzheimer's disease: A matter of blood-brain barrier dysfunction? *J. Exp. Med.* **2017**, *214* (11), 3151−3169.

(2) Zhao, Z.; Nelson, A. R.; Betsholtz, C.; Zlokovic, B. V. Establishment and Dysfunction of the Blood-Brain Barrier. *Cell* **2015**, *163* (5), 1064−1078.

(3) Zlokovic, B. V. Neurovascular pathways to neurodegeneration in Alzheimer's disease and other disorders. *Nat. Rev. Neurosci.* **2011**, *12* (12), 723−738.

(4) Wardlaw, J. M.; Smith, C.; Dichgans, M. Mechanisms of sporadic cerebral small vessel disease: insights from neuroimaging. *Lancet Neurol.* **2013**, *12* (5), 483−497.

(5) O'Brien, J. T.; Thomas, A. Vascular dementia. *Lancet* **2015**, *386* (10004), 1698−1706.

(6) Wong, S. M.; Jansen, J. F. A.; Zhang, C. E.; Hoff, E. I.; Staals, J.; van Oostenbrugge, R. J.; Backes, W. H. Blood-brain barrier impairment and hypoperfusion are linked in cerebral small vessel disease. *Neurology* **2019**, *92* (15), e1669−e1677.

(7) Zhang, C. E.; Wong, S. M.; Uiterwijk, R.; Backes, W. H.; Jansen, J. F. A.; Jeukens, C.; van Oostenbrugge, R. J.; Staals, J. Blood-brain barrier leakage in relation to white matter hyperintensity volume and cognition in small vessel disease and normal aging. *Brain Imaging Behav.* **2019**, *13* (2), 389−395.

(8) Sweeney, M. D.; Zhao, Z.; Montagne, A.; Nelson, A. R.; Zlokovic, B. V. Blood-Brain Barrier: From Physiology to Disease and Back. *Physiol. Rev.* **2019**, *99* (1), 21−78.

(9) Langen, U. H.; Ayloo, S.; Gu, C. Development and Cell Biology of the Blood-Brain Barrier. *Annu. Rev. Cell Dev. Biol.* **2019**, *35*, 591−613.

(10) Andjelkovic, A. V.; Situ, M.; Citalan-Madrid, A. F.; Stamatovic, S. M.; Xiang, J.; Keep, R. F. Blood-Brain Barrier Dysfunction in Normal Aging and Neurodegeneration: Mechanisms, Impact, and Treatments. *Stroke* **2023**, *54* (3), 661−672.

(11) Iadecola, C. The Pathobiology of Vascular Dementia. *Neuron* **2013**, *80* (4), 844−866.

(12) Tchalla, A. E.; Wellenius, G. A.; Sorond, F. A.; Gagnon, M.; Iloputaife, I.; Travison, T. G.; Dantoine, T.; Lipsitz, L. A. Elevated Soluble Vascular Cell Adhesion Molecule-1 Is Associated With Cerebrovascular Resistance and Cognitive Function. *J. Gerontol., Ser. A* **2016**, *72* (4), glw099−566.

(13) Walpola, P. L.; Gotlieb, A. I.; Cybulsky, M. I.; Langille, B. L. Expression of ICAM-1 and VCAM-1 and monocyte adherence in arteries exposed to altered shear stress. *Arterioscler. Thromb. Vasc. Biol.* **1995**, *15* (1), 2−10.

(14) (a) Matsuyama, H.; Shindo, A.; Shimada, T.; Yata, K.; Wakita, H.; Takahashi, R.; Tomimoto, H. Chronic cerebral hypoperfusion activates AIM2 and NLRP3 inflammasome. *Brain Res.* **2020**, *1736*, 146779. (b) Poh, L.; Sim, W. L.; Jo, D. G.; Dinh, Q. N.; Drummond, G. R.; Sobey, C. G.; Chen, C. L.; Lai, M. K. P.; Fann, D. Y.; Arumugam, T. V. The role of inflammasomes in vascular cognitive impairment. *Mol. Neurodegener.* **2022**, *17* (1), 4.

(15) Fassbender, K.; Bertsch, T.; Mielke, O.; Mühlhauser, F.; Hennerici, M. Adhesion Molecules in Cerebrovascular Diseases. *Stroke* **1999**, *30* (8), 1647−1650.

(16) Wettschureck, N.; Strilic, B.; Offermanns, S. Passing the Vascular Barrier: Endothelial Signaling Processes Controlling Extravasation. *Physiol. Rev.* **2019**, *99* (3), 1467−1525.

(17) Huang, J.; Li, J.; Feng, C.; Huang, X.; Wong, L.; Liu, X.; Nie, Z.; Xi, G. Blood-Brain Barrier Damage as the Starting Point of Leukoaraiosis Caused by Cerebral Chronic Hypoperfusion and Its Involved Mechanisms: Effect of Agrin and Aquaporin-4. *BioMed Res. Int.* **2018**, *2018*, 1−10.

(18) Sun, Z.; Gao, C.; Gao, D.; Sun, R.; Li, W.; Wang, F.; Wang, Y.; Cao, H.; Zhou, G.; Zhang, J.; et al. Reduction in pericyte coverage leads to blood-brain barrier dysfunction via endothelial transcytosis following chronic cerebral hypoperfusion. *Fluids Barriers CNS* **2021**, *18* (1), 21.

(19) Sun, R.; Shang, J.; Yan, X.; Zhao, J.; Wang, W.; Wang, W.; Li, W.; Gao, C.; Wang, F.; Zhang, H.; et al. VCAM1 Drives Vascular Inflammation Leading to Continuous Cortical Neuronal Loss Following Chronic Cerebral Hypoperfusion. *J. Alzheimer's Dis.* **2023**, *91* (4), 1541−1555.

(20) Zlokovic, B. V. The blood-brain barrier in health and chronic neurodegenerative disorders. *Neuron* **2008**, *57* (2), 178−201.

(21) Haley, M. J.; Lawrence, C. B. The blood-brain barrier after stroke: Structural studies and the role of transcytotic vesicles. *J. Cereb. Blood Flow Metab. Suppl.* **2017**, *37* (2), 456−470.

(22) (a) Lebel, C.; Deoni, S. The development of brain white matter microstructure. *Neuroimage* **2018**, *182*, 207−218. (b) Filley, C. M.; Fields, R. D. White matter and cognition: making the connection. *J. Neurophysiol.* **2016**, *116* (5), 2093−2104.

(23) (a) Liu, H.; Yang, Y.; Xia, Y.; Zhu, W.; Leak, R. K.; Wei, Z.; Wang, J.; Hu, X. Aging of cerebral white matter. *Ageing Res. Rev.* **2017**, *34*, 64−76. (b) Foerster, S.; Hill, M. F. E.; Franklin, R. J. M. Diversity in the oligodendrocyte lineage: Plasticity or heterogeneity? *Glia* **2019**, *67*, 1797.

(24) (a) Boggs, J. M. Myelin basic protein: a multifunctional protein. *Cell. Mol. Life Sci.* **2006**, *63* (17), 1945−1961. (b) Bagheri, H.; Friedman, H.; Siminovitch, K. A.; Peterson, A. C. Transcriptional regulators of the Golli/myelin basic protein locus integrate additive and stealth activities. *PLoS Genet.* **2020**, *16* (8), No. e1008752.

(25) Zmira, O.; Halpern, A. I.; Drori, T. Anti-neurofilament antibodies and neurodegeneration: Markers and generators. *J. Neuroimmunol.* **2020**, *344*, 577248.

(26) Su, E. J.; Fredriksson, L.; Geyer, M.; Folestad, E.; Cale, J.; Andrae, J.; Gao, Y.; Pietras, K.; Mann, K.; Yepes, M.; et al. Activation of PDGF-CC by tissue plasminogen activator impairs blood-brain barrier integrity during ischemic stroke. *Nat. Med.* **2008**, *14* (7), 731−737.

(27) Gorelick, P. B.; Scuteri, A.; Black, S. E.; DeCarli, C.; Greenberg, S. M.; Iadecola, C.; Launer, L. J.; Laurent, S.; Lopez, O. L.; Nyenhuis, D.; et al. Vascular Contributions to Cognitive Impairment and Dementia. *Stroke* **2011**, *42* (9), 2672−2713.

(28) (a) Sabayan, B.; Jansen, S.; Oleksik, A. M.; van Osch, M. J. P.; van Buchem, M. A.; van Vliet, P.; de Craen, A. J. M.; Westendorp, R. G. J. Cerebrovascular hemodynamics in Alzheimer's disease and vascular dementia: A meta-analysis of transcranial Doppler studies. *Ageing Res. Rev.* **2012**, *11* (2), 271−277. (b) Fu, P.; Chen, Y.; Wu, M.; Bao, B.; Yin, X.; Chen, Z.; Zhang, M. Effect of ferroptosis on chronic cerebral hypoperfusion in vascular dementia. *Exp. Neurol.* **2023**, *370*, 114538.

(29) (a) Ruitenberg, A.; den Heijer, T.; Bakker, S. L. M.; van Swieten, J. C.; Koudstaal, P. J.; Hofman, A.; Breteler, M. M. B. Cerebral hypoperfusion and clinical onset of dementia: The Rotterdam study. *Ann. Neurol.* **2005**, *57* (6), 789−794. (b) Venkat, P.; Chopp, M.; Chen, J. Models and mechanisms of vascular dementia. *Exp. Neurol.* **2015**, *272*, 97−108.

https://doi.org/10.1021/acschemneuro.4c00039
ACS Chem. Neurosci. 2024, 15, 2028−2041

(30) (a) Blanchette, M.; Daneman, R. Formation and maintenance of the BBB. *Mech. Dev.* **2015**, *138*, 8−16. (b) Chow, B. W.; Gu, C. The molecular constituents of the blood-brain barrier. *Trends Neurosci.* **2015**, *38* (10), 598−608.
(31) Yang, Y.; Rosenberg, G. A. Blood-brain barrier breakdown in acute and chronic cerebrovascular disease. *Stroke* **2011**, *42* (11), 3323−3328.
(32) Merlini, M.; Rafalski, V. A.; Rios Coronado, P. E.; Gill, T. M.; Ellisman, M.; Muthukumar, G.; Subramanian, K. S.; Ryu, J. K.; Syme, C. A.; Davalos, D.; et al. Fibrinogen Induces Microglia-Mediated Spine Elimination and Cognitive Impairment in an Alzheimer's Disease Model. *Neuron* **2019**, *101* (6), 1099−1108.e6.
(33) Senatorov, V. V.; Friedman, A. R.; Milikovsky, D. Z.; Ofer, J.; Saar-Ashkenazy, R.; Charbash, A.; Jahan, N.; Chin, G.; Mihaly, E.; Lin, J. M.; et al. Blood-brain barrier dysfunction in aging induces hyperactivation of TGFβ signaling and chronic yet reversible neural dysfunction. *Sci. Transl. Med.* **2019**, *11* (521), No. eaaw8283.
(34) Nation, D. A.; Sweeney, M. D.; Montagne, A.; Sagare, A. P.; D'Orazio, L. M.; Pachicano, M.; Sepehrband, F.; Nelson, A. R.; Buennagel, D. P.; Harrington, M. G.; et al. Blood-brain barrier breakdown is an early biomarker of human cognitive dysfunction. *Nat. Med.* **2019**, *25* (2), 270−276.
(35) Montagne, A.; Barnes, S. R.; Sweeney, M. D.; Halliday, M. R.; Sagare, A. P.; Zhao, Z.; Toga, A. W.; Jacobs, R. E.; Liu, C. Y.; Amezcua, L.; et al. Blood-brain barrier breakdown in the aging human hippocampus. *Neuron* **2015**, *85* (2), 296−302.
(36) Rajani, R. M.; Quick, S.; Ruigrok, S. R.; Graham, D.; Harris, S. E.; Verhaaren, B. F. J.; Fornage, M.; Seshadri, S.; Atanur, S. S.; Dominiczak, A. F.; et al. Reversal of endothelial dysfunction reduces white matter vulnerability in cerebral small vessel disease in rats. *Sci. Transl. Med.* **2018**, *10* (448), No. eaam9507.
(37) Bailey, E. L.; Smith, C.; Sudlow, C. L.; Wardlaw, J. M. Is the spontaneously hypertensive stroke prone rat a pertinent model of sub cortical ischemic stroke? A systematic review. *Int. J. Stroke* **2011**, *6* (5), 434−444.
(38) Chen, X.; Chen, L.; Lin, G.; Wang, Z.; Kodali, M. C.; Li, M.; Chen, H.; Lebovitz, S. G.; Ortyl, T. C.; Li, L.; et al. White matter damage as a consequence of vascular dysfunction in a spontaneous mouse model of chronic mild chronic hypoperfusion with eNOS deficiency. *Mol. Psychiatr.* **2022**, *27* (11), 4754−4769.
(39) Bagi, Z.; Kroenke, C. D.; Fopiano, K. A.; Tian, Y.; Filosa, J. A.; Sherman, L. S.; Larson, E. B.; Keene, C. D.; Degener O'Brien, K.; Adeniyi, P. A.; et al. Association of cerebral microvascular dysfunction and white matter injury in Alzheimer's disease. *Geroscience* **2022**, *44* (4), 1−14.
(40) Zhao, Y.; Gong, C. X. From chronic cerebral hypoperfusion to Alzheimer-like brain pathology and neurodegeneration. *Cell. Mol. Neurobiol.* **2015**, *35* (1), 101−110.
(41) Vesely, B.; Rektor, I. The contribution of white matter lesions (WML) to Parkinson's disease cognitive impairment symptoms: A critical review of the literature. *Parkinsonism Relat. Disorders* **2016**, *22*, S166−S170.
(42) Filley, C. M.; Fields, R. D. White matter and cognition: making the connection. *J. Neurophysiol.* **2016**, *116* (5), 2093−2104.
(43) (a) Kasahara, H.; Ikeda, M.; Nagashima, K.; Fujita, Y.; Makioka, K.; Tsukagoshi, S.; Yamazaki, T.; Takai, E.; Sanada, E.; Kobayashi, A.; et al. Deep White Matter Lesions Are Associated with Early Recognition of Dementia in Alzheimer's Disease. *J. Alzheimer's Dis.* **2019**, *68* (2), 797−808. (b) Wang, T.; Jin, A.; Fu, Y.; Zhang, Z.; Li, S.; Wang, D.; Wang, Y. Heterogeneity of White Matter Hyperintensities in Cognitively Impaired Patients With Cerebral Small Vessel Disease. *Front. Immunol.* **2021**, *12*, 803504.
(44) Deramecourt, V.; Slade, J. Y.; Oakley, A. E.; Perry, R. H.; Ince, P. G.; Maurage, C. A.; Kalaria, R. N. Staging and natural history of cerebrovascular pathology in dementia. *Neurology* **2012**, *78* (14), 1043−1050.
(45) Sun, Z.; Gao, C.; Gao, D.; Sun, R.; Li, W.; Wang, F.; Wang, Y.; Cao, H.; Zhou, G.; Zhang, J.; et al. Reduction in pericyte coverage leads to blood-brain barrier dysfunction via endothelial transcytosis following chronic cerebral hypoperfusion. *Fluids Barriers CNS* **2021**, *18* (1), 21.
(46) Shibata, M.; Ohtani, R.; Ihara, M.; Tomimoto, H. White Matter Lesions and Glial Activation in a Novel Mouse Model of Chronic Cerebral Hypoperfusion. *Stroke* **2004**, *35* (11), 2598−2603.
(47) Duarte Lobo, D.; Nobre, R. J.; Oliveira Miranda, C.; Pereira, D.; Castelhano, J.; Sereno, J.; Koeppen, A.; Castelo-Branco, M.; Pereira de Almeida, L. The blood-brain barrier is disrupted in Machado-Joseph disease/spinocerebellar ataxia type 3: evidence from transgenic mice and human post-mortem samples. *Acta Neuropathol. Commun.* **2020**, *8* (1), 152.
(48) Feng, L.; Li, B.; Cai, M.; Zhang, Z.; Zhao, Y.; Yong, S. S.; Tian, Z. Resistance exercise alleviates the prefrontal lobe injury and dysfunction by activating SESN2/AMPK/PGC-1α signaling pathway and inhibiting oxidative stress and inflammation in mice with myocardial infarction. *Exp. Neurol.* **2023**, *370*, 114559.
(49) (a) Hao, P.; Duan, H.; Hao, F.; Chen, L.; Sun, M.; Fan, K. S.; Sun, Y. E.; Williams, D.; Yang, Z.; Li, X. Neural repair by NT3-chitosan via enhancement of endogenous neurogenesis after adult focal aspiration brain injury. *Biomaterials* **2017**, *140*, 88−102. (b) Rao, J. S.; Zhao, C.; Zhang, A.; Duan, H.; Hao, P.; Wei, R. H.; Shang, J.; Zhao, W.; Liu, Z.; Yu, J.; et al. NT3-chitosan enables de novo regeneration and functional recovery in monkeys after spinal cord injury. *Proc. Natl. Acad. Sci. U.S.A.* **2018**, *115* (24), E5595−E5604.
(50) Zhang, S.; Xie, B.; Wang, L.; Yang, H.; Zhang, H.; Chen, Y.; Wang, F.; Liu, C.; He, H. Macrophage-mediated vascular permeability via VLA4/VCAM1 pathway dictates ascites development in ovarian cancer. *J. Clin. Invest.* **2021**, *131* (3), No. e140315.
(51) Umetani, M.; Nakao, H.; Doi, T.; Iwasaki, A.; Ohtaka, M.; Nagoya, T.; Mataki, C.; Hamakubo, T.; Kodama, T. A novel cell adhesion inhibitor, K-7174, reduces the endothelial VCAM-1 induction by inflammatory cytokines, acting through the regulation of GATA. *Biochem. Biophys. Res. Commun.* **2000**, *272* (2), 370−374.

https://doi.org/10.1021/acschemneuro.4c00039
ACS Chem. Neurosci. 2024, 15, 2028−2041